International Journal of Mechanical Sciences 312 (2026) 111253

Contents lists available at ScienceDirect

International Journal of Mechanical Sciences

journal homepage: www.elsevier.com/locate/ijmecsci

Inverse multi-objective design of three-dimensional plate-based heterogeneous mechanical metamaterials

Ramin Yousefi-Nooraie [a], Nima Razavi [b], Filippo Berto [c], Mario Guagliano [a], Sara Bagherifard [a,*]

[a] Department of Mechanical Engineering, Politecnico di Milano, Milano, Italy
[b] Department of Mechanical and Industrial Engineering, Norwegian University of Science and Technology, Trondheim, Norway
[c] Department of Chemical Engineering, Materials and Environment, Sapienza University of Rome, Rome, Italy

ARTICLE INFO

Keywords:
Energy absorption
Heterogeneous structures
Inverse design
Plate-based lattice
Deep neural network

ABSTRACT

Energy-absorbing architected metamaterials, featuring dissimilar sub-elements arranged in deliberate patterns, can achieve a notably wider array of mechanical properties compared to their uniform counterparts. The traditional design of these heterogeneous structures typically depends on expert knowledge and requires considerable trial-and-error effort. Here, we introduce a data-efficient approach for the inverse multi-objective design of high-energy absorbing, three-dimensional, heterogeneous mechanical metamaterials comprised of the combination of two distinct plate-based unit cell topologies. This approach proposes a framework that pairs a Deep Neural Network (DNN) with a Genetic Algorithm (GA), supported by finite element (FE) simulations, to inverse design heterogeneous metamaterials with tailored Young's modulus (E), while maximizing energy absorption capacity and minimizing relative density (ρ). We applied this method to orthopaedic implants, as a case study, to design structures with a desirable biocompatible elastic modulus, enhanced energy absorption efficiency and minimized ρ. To the best of our knowledge, this is the first inverse design framework that integrates clustering-aware deep neural networks with evolutionary optimization, enabling accurate and efficient design of heterogeneous plate-based lattices with tailored mechanical performance.

1. Introduction

Lattice and cellular structures have attracted growing attention in recent years due to their exceptional mechanical performance and versatility across engineering applications [1–12]. Such architectures can achieve high stiffness-to-weight ratios, tunable energy absorption, and multifunctionality, making them ideal candidates for lightweight structures, protective devices, and biomedical implants. With the rapid advances in additive manufacturing, the design space for these structures has significantly expanded, enabling the realization of complex unit cells, hierarchical features, and heterogeneous architectures that were previously infeasible [13–25].

Despite these advances, the inverse design of lattices, i.e., mapping target properties back to structural parameters, remains a formidable challenge. Conventional forward simulations or experimental trial-and-error approaches are computationally costly and scale poorly with increasing design complexity. To address this, machine learning (ML) surrogates have been developed to accelerate property prediction [26–31]. Coupled with optimization algorithms such as genetic algorithms (GAs) and evolutionary strategies, such surrogates have enabled the design of lightweight and energy-absorbing cellular structures [32–36]. More recently, deep learning and generative models have been introduced for lattice design [30,37–43], and physics-informed ML frameworks have emerged as promising alternatives [44,45]. However, these methods typically require large datasets or are restricted to homogeneous designs, narrow unit cell families, or single-objective optimization, limiting their applicability to realistic heterogeneous systems.

A particularly underexplored area is the systematic treatment of heterogeneity in lattice design. Heterogeneous lattices, where strut or plate properties vary spatially, offer opportunities for enhanced multifunctionality, but also introduce substantial challenges in capturing property–structure relationships [46,47]. To the best of our knowledge, no prior study has explicitly incorporated clustering-based descriptors to model and exploit heterogeneity effects in inverse design. Furthermore, most existing frameworks do not balance computational efficiency with accuracy when targeting multiple properties such as elastic modulus,

* Corresponding author.
E-mail address: sara.bagherifard@polimi.it (S. Bagherifard).

https://doi.org/10.1016/j.ijmecsci.2026.111253
Received 11 July 2025; Received in revised form 19 November 2025; Accepted 12 January 2026
Available online 14 January 2026

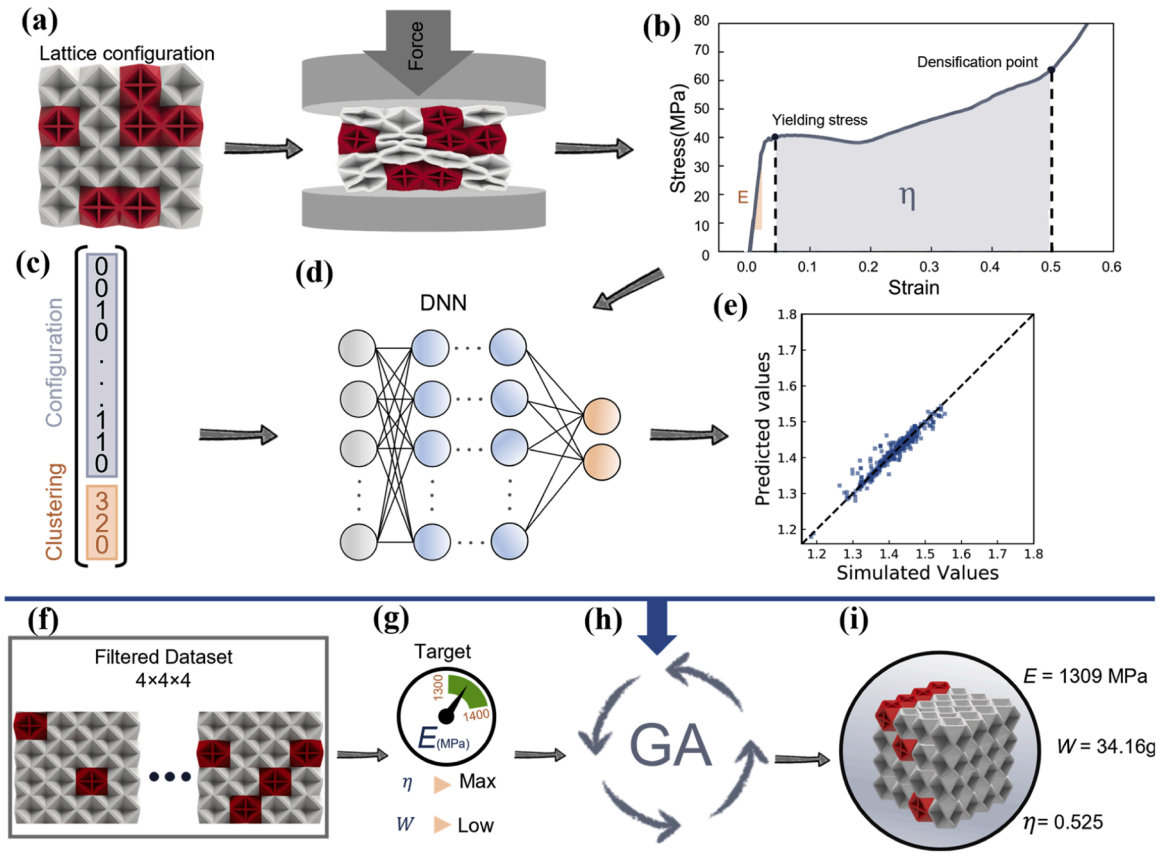

Fig. 1. Schematic illustrating the developed framework for the inverse design of heterogeneous lattice structures. **(a)** FE modelling of the quasi-static compression test for a lattice configuration consisting of two distinct unit cell topologies. **(b)** Extraction of elastic modulus (E) and energy absorption efficiency (η) from the FE simulation result. **(c)** Vectorization of the input data to a DNN model by combining configuration and clustering data. **(d)** Using the DNN model to predict E and η. **(e)** Comparison of the DNN model predictions and the FE simulation results. **(f)** Identifying the configurations to be filtered within the design space. **(g)** Assessing the results in terms of η and ρ, considering the boundary conditions (E range). **(h)** Using the fitness function of the GA to identify the best candidate considering the design requirements. **(i)** Uncovering the best design.

yield strength, and energy absorption simultaneously.

In this work, we propose a novel hybrid framework that integrates deep neural networks (DNNs) with genetic algorithms (GAs) for the inverse design of heterogeneous plate-based lattices (see Fig. 1). Our approach introduces clustering descriptors to explicitly account for heterogeneity, enabling accurate prediction and optimization of complex property relationships. Importantly, the framework achieves high accuracy with relatively small datasets, avoiding the prohibitive computational cost associated with large-scale generative or physics-informed approaches [48–51]. This combination of clustering-awareness and computational efficiency allows us to design lightweight structures with tailored trade-offs between stiffness and energy absorption, offering new possibilities for practical lattice applications.

The remainder of this paper is organized as follows: Section 2 presents the problem definition and outlines the proposed inverse design framework, including the unit cell selection, mechanical targets, and simulation setup. Section 3 describes the training and validation of the deep learning model and details the implementation of the genetic algorithm for optimization. In Section 4, we present and discuss the results of the inverse design, including the analysis of the top-performing configurations and the identification of effective structural motifs. Finally, Section 5 summarizes the key conclusions and outlines potential directions for future research.

2. Materials and methods

This section presents the full methodology behind the proposed inverse multi-objective design framework. We begin by formulating the design problem within a biomedical context, specifically targeting bone scaffolding applications. The mechanical targets, material selection rationale, and design objectives are first established. We then (as shown in Fig. 1) detail the construction of the design space, including unit cell selection, configuration strategy, and finite element (FE) simulation setup for mechanical property extraction. Experimental validation is provided to ensure the fidelity of the simulation approach. Next, we describe the data preprocessing and machine learning pipeline, including the development and training of a deep neural network (DNN) to predict key mechanical properties. Finally, we outline the genetic algorithm (GA)-based inverse design process used to identify optimal configurations that satisfy mechanical constraints while maximizing energy absorption and minimizing relative density.

2.1. Multi-objective problem

The developed framework was used to tackle the bone scaffolding problem in the biomedical field, as a case study to demonstrate the efficiency of the proposed design approach. The characteristics of the bone are not easily predictable and could differ based on multiple factors, including age, gender, bone composition, race, and bone site in the human body. Bone structure is generally categorized into cortical and cancellous macroscopic forms, with E of the cortical bone reaching 30 GPa, while that of the cancellous bone can vary between 0.02 and 2 GPa [52]. Whilst the natural bone tissue has a significant healing ability in the case of minor defects, critical-size bone defects cannot be spontaneously healed and require structural reinforcement to bridge the bone

gap and promote the repair process. Metals and polymers are being employed for such bone implants; however, the latter have demonstrated relatively better outcomes, primarily due to their closer mechanical properties to those of natural bone [53]. Although metals exhibit higher stability compared to polymers, they often present significantly higher stiffness than natural bone [54]; this mismatch in mechanical properties enhances the risk of stress shielding that could result in poor integration of the scaffold by impeding the remodeling process in the host bone matrix [55]. This limitation of metallic implants can be alleviated by using AM to create intricate, porous lattice structures with precisely controlled architecture offering mechanical properties that can be finely tuned to better match those of natural tissues, at a lower weight, while ensuring the required permeability for improved integration.

To demonstrate the efficiency of the developed design framework, here we consider the inverse design of a scaffold for possible implantation in the femur bone area as a representative application. We set the stiffness of our heterogeneous structure as that of the bone in the proximal femur (E ranging between 1.3 and 1.4 GPa) [56], necessary for effective load bearing and stress distribution. Subsequently, we explored the design space for the structures with the highest energy absorbance at the lowest ρ that can fulfill this E range. In this design methodology, the mechanical response of the structure is characterized by its compressive stress-strain curve and the energy absorption that would provide important insights into its load-bearing behavior. E is estimated as the slope of the linear segment in the stress-strain curve to quantify the material's resistance to external stress before permanent deformation. The yield strength (Y) is defined as the stress corresponding to 0.2 % permanent strain, indicating the onset of plastic deformation. Additionally, energy absorption efficiency (η) was considered as a critical metric reflecting the structure's capacity to deform and absorb energy before collapsing under load. It was estimated by the area under the stress-strain curve up to the densification point, a point at which the structure loses the ability to efficiently absorb energy due to the notable increase in its density [57] (see Fig. A1).

To design this structural metamaterial, we utilized 4 × 4 × 4 cubic configurations of two distinct unit cells as the model input. This specific configuration was chosen to create a balance between the level of architectural complexity and computational efficiency. The individual unit cells were selected from the plate-based topological category. This class of lattice structures, formed by arranging plates along crystal structure planes, offers uniform mechanical properties in all directions, reaching much higher E and Y in the same relative density as their counterpart strut-lattice structure with the same base topology [58], while offering a high energy absorption property under compression [59,60].

As shown in (Fig. 2), the Face-Centered Cubic (FCC) plate-based design (type-A) was selected as the base unit cell, due to its high energy absorption capacity [13]. This bending-dominated topology has been successfully used in bone scaffolding applications in the past [61]. Its energy dissipation property, combined with structural integrity, makes it an excellent choice for the discussed application. The second unit cell design comes from a combination of FCC (bending-dominated topology) with Simple Cubic (SC) (stretching-dominated topology) unit cells to create a reinforced version of the FCC topology with higher stiffness (type-B) [13]. Here we implement the developed design strategy to carefully balance the number of each of these unit cells in the final arrangement to achieve a structural configuration that would meet the requirements of stiffness (E), offering the highest energy absorption efficiency (η) at the lowest ρ.

2.2. Property prediction

The total number of possible heterogeneous design configurations in the X-Y plane is 65,536. We considered the response of the flipped configurational geometries with respect to the X-direction, Y-direction, and the combination of X and Y-direction to be identical under the quasi-static compression test [62] (Fig. 3a). After filtering out these repetitive configurations, the dataset was reduced to 16,576 unique configurations. It is worth noting that the data regarding these repeated configurations was eventually added to the input dataset to improve the accuracy of the DNN model predictions. We also limited the maximum number of reinforced unit cells (Type-B) in the configurations to 24, as structures exceeding this limit possess a higher level of Young's modulus

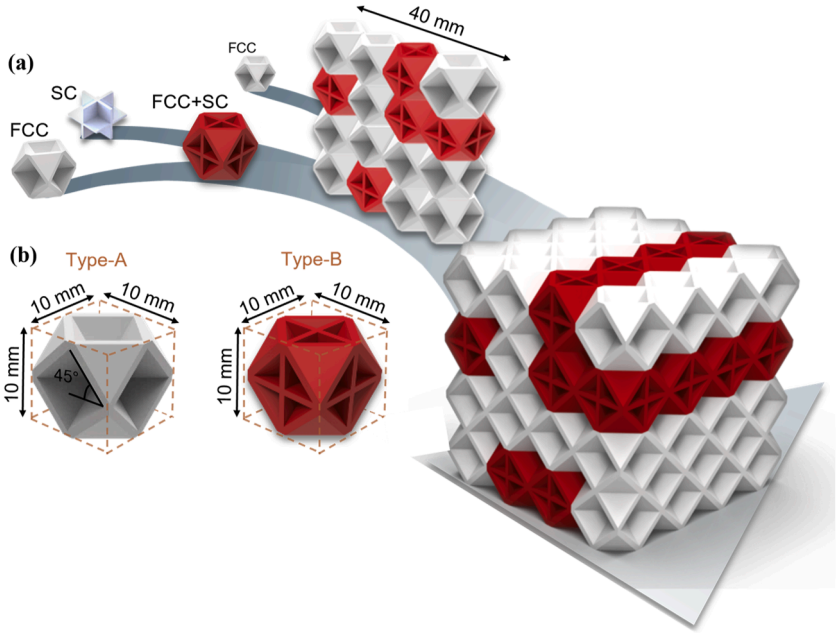

Fig. 2. Design procedure for the heterogeneous lattice configuration. The procedure of designing two distinct unit cells from the plate-lattice category. **(a)** The first unit cell is FCC plate-based design (Type-A), and the second unit cell is the result of combining FCC with SC topology (Type-B). The configurations consisting of combinations of type-A and type-B cells in a 4 × 4 stack will be created and repeated three times in the third direction. **(b)** The dimensions of type-A and type-B unit cells.

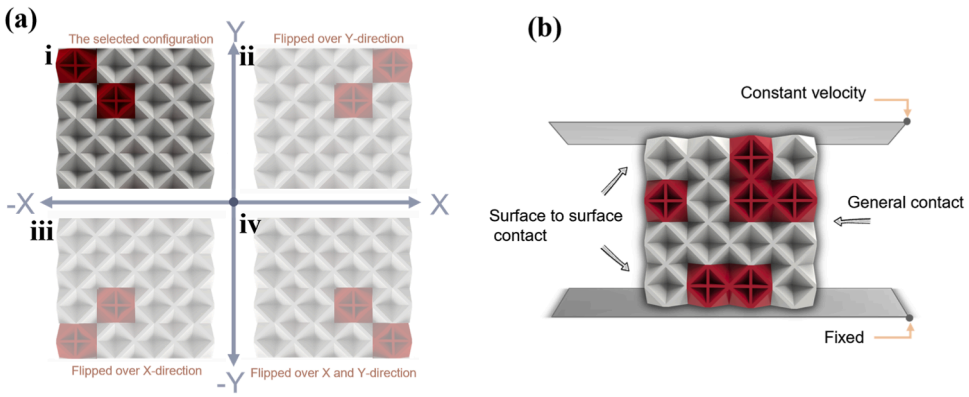

Fig. 3. Schematics depicting the screening step to filter out the flipped configurations and representing the FE model set-up. **(a)** Filtering out all possible repeated configurations: ***i*** the selected configuration ***ii*** The flipped configuration over Y-direction ***iii*** The flipped configuration over X-direction ***iv*** The flipped configuration over X and Y-direction. **(b)** The schematic showing the FE model and its the boundary conditions.

beyond the valid range of our target application for the proximal femur bone.

2.3. Finite element modeling

FE simulations were performed on a randomly selected 20 % subset of the dataset to provide input for the DL model. To speed up the simulations, a code was developed for analysis automation. The binary matrix describing the unit cell arrangements was converted into a 16-member vector to be used as input data for a custom-made Python script. As shown in (Fig. 4a), the script started with importing two previously saved models containing two uniform 4 × 4 structures, one made entirely of type-A and the other made entirely of type-B cells. The structures were then positioned exactly at the same coordinates in the XY-plane. Subsequently, the script read the binary code of the selected configuration and started scanning each cell position, using the binary key (0 for A and 1 for B) to update the configuration, selecting which one (type-A or type-B) to assign to each cell position. Once the scanning process was completed, the 16 cells (XY plane positions) of the configuration were defined in the assembly module. In the next step, a 4 × 4 × 4 lattice was created by replicating the structure three times in the Z-direction. Following this, the script created and launched the FE simulation of compression tests, saved the extracted force and displacement data, and subsequently repeated the process for the next configuration.

The FE simulations of lattice deformation under compressive loading were carried out using Abaqus Software version 2022. The structures were meshed using 3D linear tetrahedral elements (C3D4). A preliminary mesh convergence analysis (see Fig. B1) indicated that each type-A cell required approximately 4000 elements, while type-B needed around 5000 elements for accurate meshing. An elastic-perfectly plastic material model was considered, defined by the *E* and the yield stress (see Table C1) []. The lattice structure was placed between two rigid plates, with the top plate applying a downward velocity of 35 mm/s (Fig. 3b). This velocity, which is considerably higher than the one set in the experiments, was selected to reduce the computational costs. The assumption of higher displacement velocity was validated by ensuring that the kinetic energy of the FE model remained lower than 5 % of the internal energy throughout the simulation, indicating coherence with the quasi-static experimental condition. The upper plate's other degrees of freedom (DOFs) were restricted, while the bottom plate was fully constrained. Surface-to-surface contact was used at the interface of the rigid plates and the lattice, and general contact was considered for self-

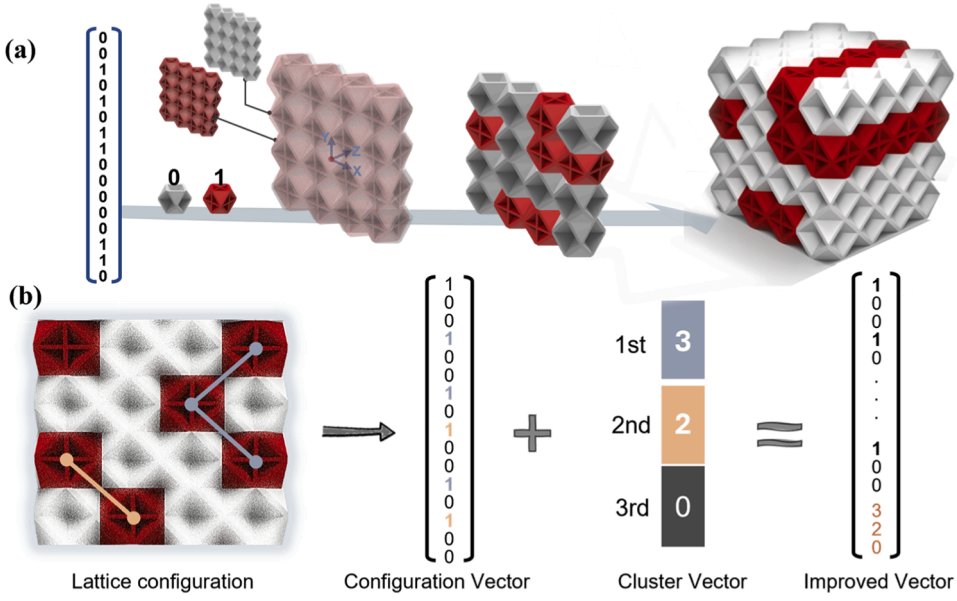

Fig. 4. Algorithms developed for automation and cluster finding. **(a)** Different steps of automated configuration generation for FE simulations. **(b)** The process of identifying directly connected type-B cells (clusters) in each configuration.

contact within the structure. A penalty contact model with a friction coefficient of 0.2 was utilized as the interaction property for the surface-to-surface and general contact.

2.4. Experimental validation

To validate the numerical model, we fabricated a number of baseline uniform lattice samples. The test specimens were manufactured via the fused deposition modeling (FDM) technique using an Original Prusa i3 MK3 printer with PLA filament (3DNet, Norge) of 1.75 mm diameter. The process parameters are summarized in Table D1.

Quasi-static compression tests were performed in accordance with the ASTM D695 standard (Standard Test Method for Compressive Properties of Rigid Plastics), which is widely adopted for polymeric and additively manufactured lattice structures. Elastic modulus and yield strength were extracted following the guidelines of this protocol to ensure consistency and reproducibility of the results. Testing was carried out on an MTS Criterion model C42 electromechanical load frame equipped with a 5 kN load cell, using a crosshead speed of 2 mm/min.

Five replicates per condition were tested. The extracted stiffness and energy absorption efficiency were compared against the corresponding FE model predictions. The results showed good agreement, with a maximum error of 11 % (see Fig. 5 and Table D1), thereby validating the reliability of the numerical data used for DNN training.

2.5. Data preparation for deep learning model

E, Y, and η for all simulated configurations were extracted to gather data for the DNN model. A Python script was developed to automatically determine E by analyzing the slope of the stress-strain diagrams within the elastic region (see Fig. A1). Then, Y was attained by identifying the intersection of the stress-strain curve with a line starting from 0.2 % strain with a slope equal to E. To assess the energy absorption capacity of the structure, η, was defined based on the uniaxial stress-strain curve, as defined in (Eq. (1)):

$$\eta(\varepsilon) = \frac{1}{\sigma(\varepsilon)} \int_0^{\varepsilon} \sigma(\varepsilon) d\varepsilon \ . \tag{1}$$

The onset of densification strain corresponds to the strain where the derivative of the η curve is zero, defined as ε_{cd}, where:

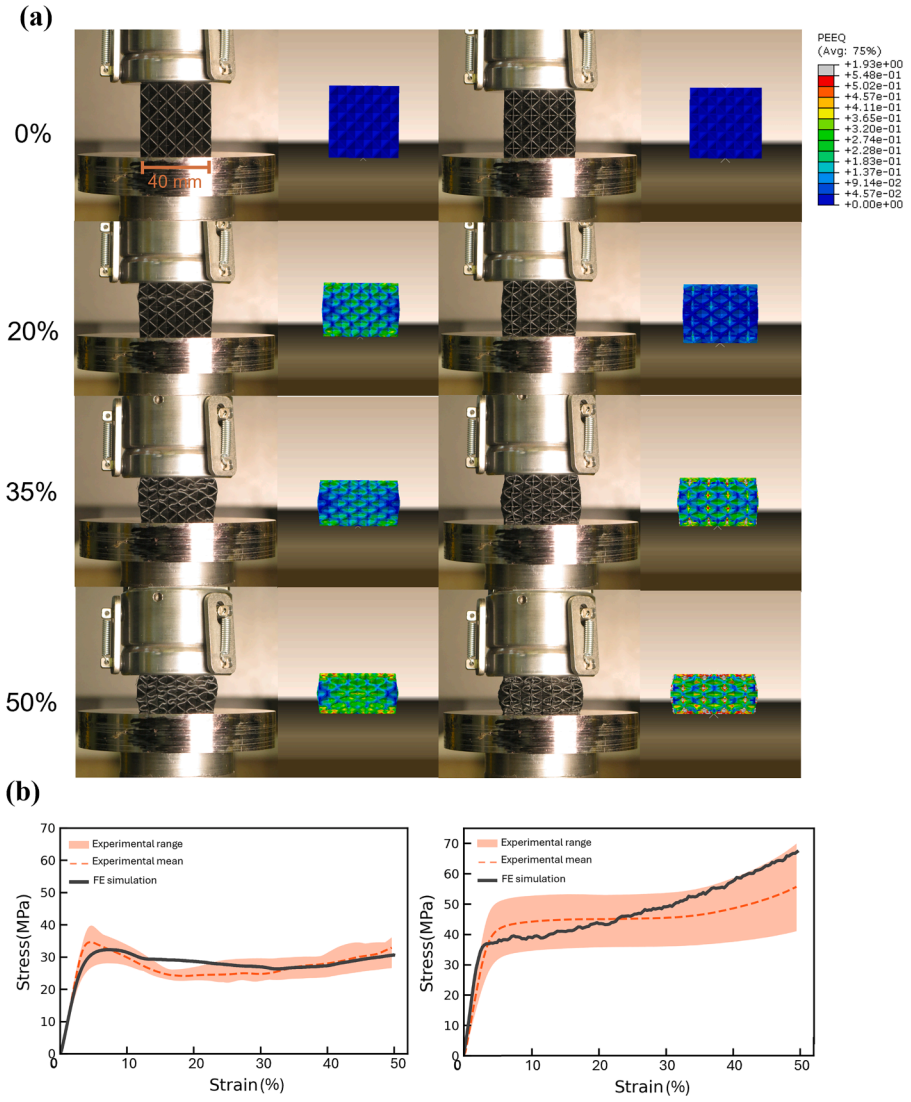

Fig. 5. Numerical Model evaluation. To validate the numerical model, we realized five samples for each configuration. The comparison between the experimental and numerical data showed good agreement. **(a)** compression test for uniform configurations up to 50 % of strain. **(b)** Comparison between experimental and numerical data for validating the FE model for creating data for DNN.

$$\left.\frac{d\eta(\varepsilon)}{d\varepsilon}\right|_{\varepsilon=\varepsilon_{cd}} = 0 \ . \tag{2}$$

Thus, ε_{cd} is the onset of densification strain where stress increases rapidly under compression loading. To exclude any recoverable energy from the calculation, (Eq. (1)) was modified as below:

$$\eta(\varepsilon) = \frac{1}{\sigma(\varepsilon)} \int_{\varepsilon_y}^{\varepsilon} \sigma(\varepsilon) d\varepsilon \ . \tag{3}$$

2.6. Deep learning model

We vectorized the configuration data to make it eligible for feeding into the DNN model. However, this would enhance the risk of losing some of the geometrical information, which is hidden inside the structure, like the direct connection between the reinforced unit cells. This loss could considerably reduce the accuracy and reliability of the model's predictions. To address this issue, we have developed an algorithm that finds interconnectivity (clusters) among the reinforced unit cells (type-B) in each configuration. As shown in (Fig. 4b), this algorithm starts scanning the structure in the XY plane from the top-left and assesses the cells around the first identified type-B unit cell by inspecting the area toward left-right and top-down. In the case that another type-B unit cell is spotted, the algorithm investigates if this candidate is in direct contact with any other similar unit cells. If true (confirming the presence of at least one cluster), it carries on the connectivity check and reports the cluster size (i.e., the number of connected unit reinforced cells). Consequently, the algorithm repeats scanning the rest of the structure line by line and searches for new type-B unit cells. A new candidate will be considered as a member of a new cluster only if it has a direct connection with at least one other type-B unit cell and does not have a connection with any member of a previously established cluster. The result will be a vector consisting of three values, each possibly ranging from 0 to 6.

We used a fully connected DNN as the predictor due to its versatility and ability to approximate any continuous function and to grasp intricate patterns and connections within the data. The initial layer comprised 19 neurons: 16 representing the binary data of (XY) unit cell arrangements and 3 for cluster characterization (ranging from 0 to 6). The output layer contained two neurons that signified E and η. To find the optimum number of hidden layers and the number of neurons in each layer, an analysis was conducted using the Keras Tuner hyperparameter optimization framework, searching a wider range of different simple and complex models to find the best model with optimized parameters. The activation function for the hidden layers was Rectified Linear Unit (ReLu), and the validation metric for the loss function was Mean Squared Error (MSE). The range of possible hidden layers was set between 2 and 20, and the number of neurons in each layer was considered between 32 and 512 with increments of 32 neurons. The learning rate varied between 0.0001 and 0.01 with logarithmic sampling. The total number of trials (configurations) was set to 20, with a maximum of 3 retries for each conducted over 100 epochs. The data were randomly split into 80 % for learning and 20 % for testing. The resulting model had 20 hidden layers with 288, 480, 192, 96, 320, 256, 128, 512, 192, 352, 64, 384, 448, 352, 384, 96, 128, 32, 416, and 32 neurons in layers, respectively. The initial learning rate of the selected model was 0.0005. The maximum number of epochs was set to 4000, with early stopping triggered if there was no further decrease in the loss function. Cross-validation was also used to monitor the validation errors. The loss function for trained and test data was monitored to prevent any overfitting for the model.

Adam optimizer was used to adjust the weights and biases using backpropagation with the initial learning rate resulting from the Keras Tuner analysis. The trained model can predict the unseen data with an R-squared factor of 93 % (92 % for E and 93 % for η), MSE of 0.012(0.014 for E and 0.010 for η), and Mean Absolute Error (MAE) of 0.007(0.008 for E and 0.006 for η).

2.7. Inverse design of the lattice configuration

Using the trained and validated DNN, we implemented a genetic algorithm (GA) to explore the design space and identify optimal configurations with higher fitness scores. The fitness function was carefully designed to evaluate and rank top-performing candidates based on their elastic modulus (E), specific energy absorption (η), and structural ρ. The goal was to detect structures with the highest possible η and minimal relative density, while ensuring that E remained within a desirable mechanical range (between 1.3 and 1.4 GPa in the current case).

$$f = \eta + \frac{3}{\log(\mathrm{W})} \text{ where } E_{min} \leq E \leq E_{max} \ . \tag{4}$$

The function f in (Eq. (4)) balances mechanical performance and lightweight design: η rewards energy absorption capacity, while the inverse logarithmic term penalizes heavier structures without excessively skewing the search toward ultralight but weak solutions. This formulation ensures that fitness improves with increasing energy absorption and decreasing ρ, but only for structures with E within the defined range, which reflects practical material constraints. The logarithmic component was chosen to avoid overly aggressive penalization of weight and to maintain a smooth optimization landscape for the GA.

The GA was executed for 50 generations, beginning with a randomized initial population and iterating through evaluation, selection, crossover, and mutation to identify the best-performing designs. Fig. 6 illustrates the convergence of the GA's fitness function during the optimization process.

3. Results and discussion

This section presents and discusses the key results of the proposed inverse design framework, focusing on the performance and spatial arrangement of the optimized 3D heterogeneous metamaterial configurations. We first evaluate the mechanical properties of the top-performing structures selected by the genetic algorithm, comparing predicted values with FE simulations to validate the model's accuracy. A broader exploration of the design space is then presented, highlighting trade-offs between stiffness, energy absorption, and ρ. The underlying structural motifs responsible for enhanced performance are analyzed in relation to their spatial arrangement and cluster orientation. Finally, the influence of various loading scenarios and potential design extensions is considered, highlighting the adaptability and potential of the framework for broader applications.

The top five structures selected by the algorithm as the best

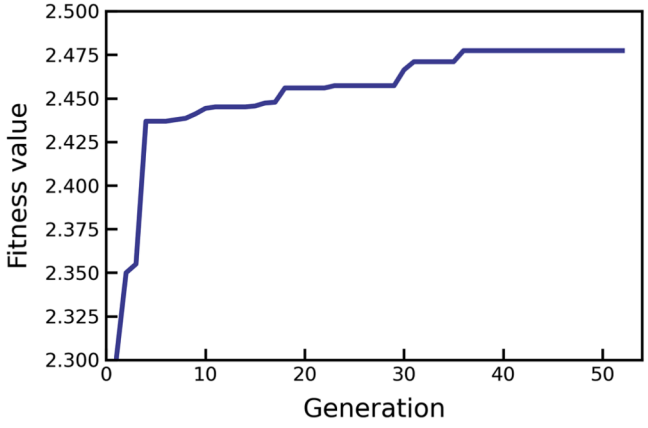

Fig. 6. Illustrates the convergence of the GA's fitness function during the optimization process.

performing candidates are shown in (Fig. 7), where the best configuration possesses an E of 1306 MPa and maximized η of 0.503.

For further validation, the numerical analysis was implemented for the five configurations selected by the GA and the results were compared to the predicted DNN values. This comparison, as shown in (Fig. 8) indicates a close coherence between the predicted and simulated outcomes.

This work demonstrates a multi-objective deep learning-based approach for inverse design of additively manufactured 3D architected heterogeneous metamaterials with customizable mechanical properties.

(Fig. 9) shows a contour plot based on the computed weight(W) as a function of E and η, which presents the dispersion map of the configurations within the dataset, considering the two uniform structures (consisting of only type-A and only type-B unit cells) as reference. The top five configurations identified by the GA are also indicated on the map. It is to be noted that the irregular shape of the contour map arises from the interpolation of discrete FE data points, each corresponding to a specific lattice configuration. This irregularity highlights the inherent nonlinearity between elastic modulus and energy absorption efficiency.

To better describe the selection process and evaluate the possible promising patterns, a series of top five arrangements suggested by the algorithm were extracted for four different ranges of E, starting from 1.1 up to 1.5 GPa with intervals of 0.1 GPa, as shown in (Fig. 10). The algorithm yields the configurations with the highest η within the imposed E range. However, for two configurations with similar η range, it will assign a higher fitness value to the structure with the lower ρ among the two. As an example, C-ii is ranked higher compared to C-iii, since it weighs less, although it has a slightly lower η (also see D-ii and D-iii).

The initial observation of the results, for identifying the underlying patterns leading to enhanced performance (within the criteria set for this specific case study), shows that by increasing the number of reinforced unit cells (type-B), the overall stiffness increases while η exhibits a decreasing pattern. However, other parameters like the arrangement of the reinforcements can also highly affect the E. The results indicate that lattice structures with clustered reinforced cells tend to exhibit higher E (B-ii, C-i, and C-iv). As shown in C-i, C-ii, D-i, D-ii, and D-iii, arranging the clusters in vertical orientation has a more notable effect on E compared to the clusters arranged horizontally or diagonally. Hence, the highest E in the analyzed configurations belongs to the D-iii, which contains five reinforced cells all clustered together, with three of the members forming a vertical cluster. Furthermore, the results suggest that a vertical arrangement of type-B unit cells in every horizontal layer of the structure would drastically limit the overall deformability of the lattice structure under compressive loading. These observations are valid when the cluster is formed along the loading direction.

In terms of η, two general trends emerge from the results. First, by increasing the number of reinforced cells, the η would decrease. This trend was predictable since by adding more unit cells that possess stretching-dominating properties, the ability of the structure to deform will decrease, resulting in a decline in η. Secondly, the η of the lattice structures highly relies on the number of type-B unit cells as well as their arrangement. The most prominent design pattern for a structure with the targeted E and high η is to arrange the reinforced unit cells within the lattice structure in a way to increase the plateau region after the yielding point and achieve higher densification strain. This objective can be achieved by dispersing the type-B unit cells within the structure in different horizontal layers, preferably with no cluster or short horizontal or diagonal clusters, as the reinforced cells' scattered distribution seems to increase the overall energy absorption capacity of the integrated structure. These arrangements would help the lattice to deform up to a higher strain level before reaching the densification point, resulting in an overall higher η.

The use of uniform compression in this study provided a consistent and controlled baseline for validating the inverse design framework, enabling a clear examination of how topological arrangement can influence stiffness and energy absorption. Although real orthopedic applications may involve non-uniform or site-specific loading, the proposed DNN–GA architecture can be adopted to such cases as it is not constrained by the loading condition considered in this study. By retraining the surrogate model on FE data representing spatially varying or anisotropic stress fields, the framework can be adapted to more complex, anatomically realistic scenarios. This flexibility highlights its potential for future extension to more specific patient-specific applications.

In case the loading direction changes from vertical to horizontal, these identified motifs will remain valid as long as the correlation between the reinforced cells' arrangement and the loading direction is taken into account. However, under biaxial pressure, the motifs will not be effective. For instance, C-i and C-ii are the best options under uniaxial loading, but their configuration will not necessarily show the best performance under biaxial pressure. Under biaxial pressure, B-iii could be a better candidate due to its comparable properties in both horizontal and vertical directions. Although designed for uniaxial pressure, the framework can be adapted to predict the best performing configurations also for bi-axial pressure, if trained using corresponding data.

In this study, we limited the lattice size to a 4 × 4 in-plane configuration and adopted a quasi-3D setup with identical repetition along the Z axis. These choices were made to balance computational efficiency and experimental feasibility, enabling us to clearly demonstrate the capabilities of the proposed clustering-aware DNN + GA framework. However, these constraints are not inherent to the methodology. The framework can be scaled to larger or irregular domains, and the GA

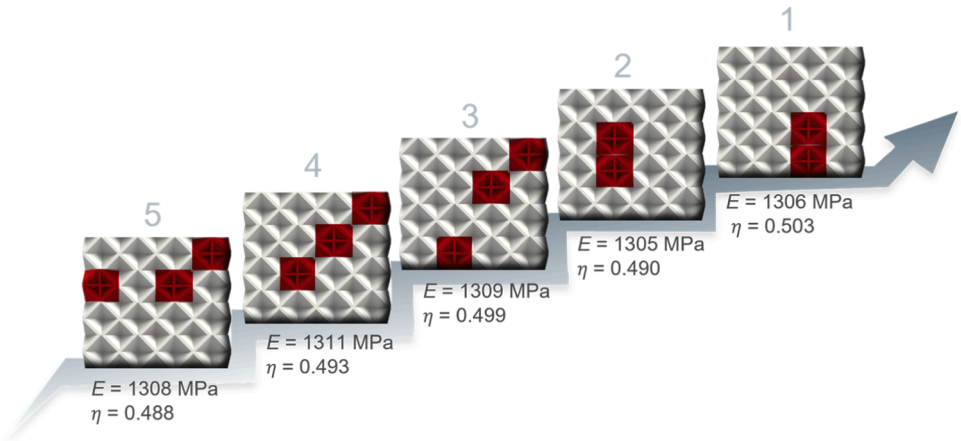

Fig. 7. Selected structural configurations based the design requirements of the case study. From left to right the top five candidates selected by the algorithm based on the design requirements.

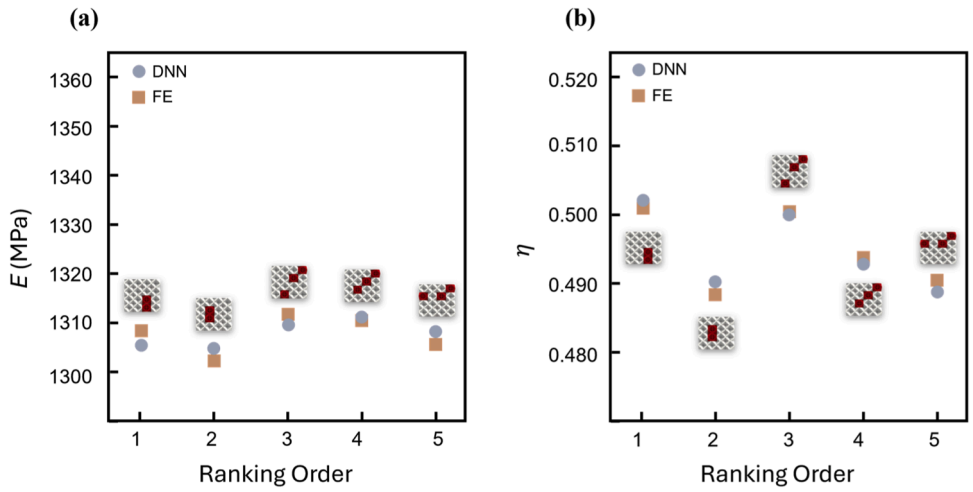

Fig. 8. Comparison of the GA's top five configurations' E and η with the corresponding numerical data. **(a)** comparison of the *E* form numerical modeling and the DNN prediction. **(b)** comparison of the η form numerical modeling and the DNN prediction.

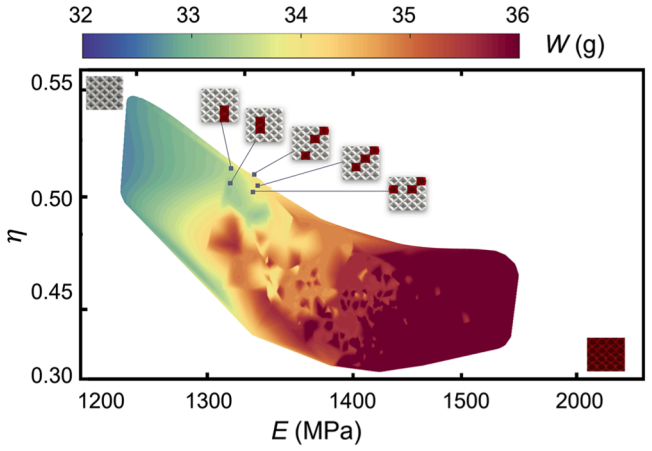

Fig. 9. Contour plot based on the computed weight (*W*) as a function of *E* and η.

optimization stage is not restricted to fixed dimensions. Likewise, the DNN surrogate can be retrained for fully 3D heterogeneous configurations, which would significantly expand the accessible design space. Exploring these extensions represents a natural direction for future work and highlights the adaptability of our approach.

The proposed framework demonstrated a strong capability to tailor the mechanical response of heterogeneous lattices. As illustrated in Fig. 9, the optimized configurations are able to cover a substantial range in both elastic modulus (~1200–2000 MPa) and energy absorption efficiency (~0.33–0.55), confirming the framework's sensitivity to topological variations. Importantly, this adaptability stems from the framework's independence from any specific unit cell topology; altering the base topologies would directly reshape the property landscape explored by the GA. This highlights the method's versatility and efficiency, showing that its performance is governed by the intrinsic mechanical characteristics of the selected unit cells rather than by computational constraints.

It is important to note that this behavior does not represent a limitation of the proposed inverse design framework but rather reflects the characteristics of the chosen base topologies. The developed DNN–GA framework is fully adaptable and topology-independent: by selecting alternative unit cells, it can present configurations with delayed densification and extended crushing distances, thereby achieving even higher energy absorption efficiency.

As a natural extension, future work could explicitly incorporate the effect of building orientation and feature size on mechanical anisotropy by parametrizing the deposition direction in the FE simulations and training data, to allow orientation- and size-dependent predictions and further generalization of the design rules.

In this study, the geometrical affinity of the two selected building blocks significantly minimized the likelihood of stress concentration at the interfaces of adjacent unit cells; this design aspect plays a crucial role in the structure's overall strength. Future developments could involve introducing a higher number of geometrical variables, such as implementing gradients in thickness [63]. While this increases the complexity of the FE model and computational costs, it enhances the inclusiveness of the design framework, leading to a higher level of customizability.

4. Conclusion

In this work, we presented a data-efficient, deep learning-assisted inverse design framework for the creation of heterogeneous 3D plate-based lattice structures, tailored to the mechanical requirements of biomedical bone scaffolding applications. By integrating stretching- and bending-dominated unit cells into architected 4 × 4 × 4 lattices, we addressed the critical challenge of matching implant stiffness to that of native bone while maximizing energy absorption and minimizing ρ.

To enable accurate prediction across a vast design space, we combined finite element simulations with experimental validation and introduced a cluster-detection algorithm that preserved key topological information during model vectorization. This enhancement significantly improved the performance of the fully connected deep neural network, which achieved coefficient of determination values exceeding 92 % for both stiffness and energy absorption predictions.

Coupling the trained model with a genetic algorithm enabled efficient navigation of the design space, yielding optimal scaffold configurations with target-level stiffness, superior energy dissipation, and lightweight characteristics suitable for proximal femur implantation. This outcome demonstrates the power of combining interpretable design metrics with machine learning and evolutionary search for inverse structural design.

The proposed framework is generalizable and scalable, offering a practical pathway toward the design of next-generation metamaterials and scaffolds that must meet multi-objective performance constraints. While developed for orthopedic applications, the methodology can be extended to other domains, such as aerospace, protective systems, and soft robotics, where precise control of mechanical behavior and manufacturability are essential.

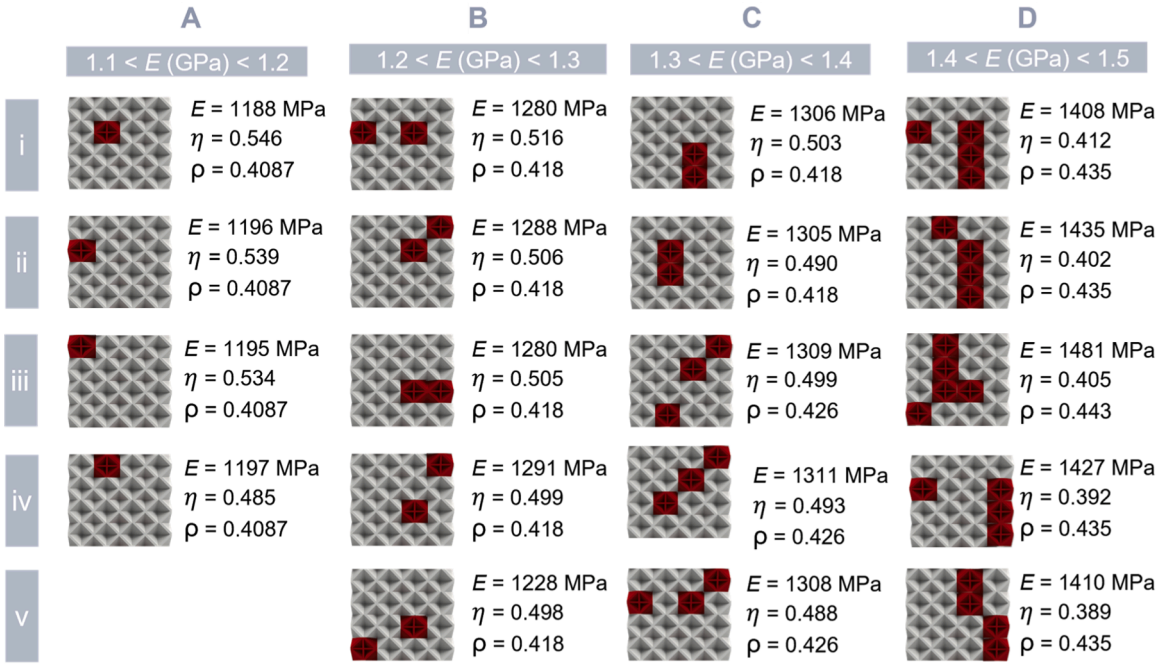

Fig. 10. Analysis of possible motifs and patterns among the best-performing designed heterogeneous lattice structures. Illustration of the five best candidates for four different ranges of *E*.

CRediT authorship contribution statement

Ramin Yousefi-Nooraie: Writing – original draft, Visualization, Validation, Software, Methodology, Investigation, Formal analysis, Data curation, Conceptualization. **Nima Razavi:** Writing – review & editing, Resources, Methodology, Investigation. **Filippo Berto:** Writing – review & editing, Methodology. **Mario Guagliano:** Writing – review & editing, Supervision. **Sara Bagherifard:** Writing – review & editing, Supervision, Methodology, Funding acquisition, Conceptualization.

Declaration of competing interest

The authors declare that they have no known competing financial interests or personal relationships that could have appeared to influence the work reported in this paper.

Acknowledgements

This research received funding from the European Research Council (ERC) under the European Union's Horizon 2021 research and innovation programme (ArcHIDep ERC—Co project, grant agreement n. 101044228). Views and opinions expressed are however those of the author(s) only and do not necessarily reflect those of the European Union or the European Research Council Executive Agency. Neither the European Union nor the granting authority can be held responsible for them.

Supplementary materials

Supplementary material associated with this article can be found, in the online version, at doi:10.1016/j.ijmecsci.2026.111253.

Data availability

The link to the data used is included in the manuscript.

References

[1] Ejeh CJ, Barsoum I, Abu Al-Rub RK. Impact behavior of periodic, stochastic, and anisotropic minimal surface-lattice sandwich structures. Int J Mech Sci 2024;276:109359. https://doi.org/10.1016/j.ijmecsci.2024.109359.
[2] Daynes S, Feih S. Functionally graded lattice structures with tailored stiffness and energy absorption. Int J Mech Sci 2025;285:109861. https://doi.org/10.1016/j.ijmecsci.2024.109861.
[3] Wang Y, Chen X, Sun Y, Zhang J, Hu J, Bai L. Full-band vibration isolation and energy absorption via cuttlebone-inspired lattice structures. Int J Mech Sci 2024;274:109283. https://doi.org/10.1016/j.ijmecsci.2024.109283.
[4] Liu X, Wang Y, Liu X, Ren Y, Jiang H. Synergetic control mechanism for enhancing energy-absorption of 3D-printed lattice structures. Int J Mech Sci 2024;262:108711. https://doi.org/10.1016/j.ijmecsci.2023.108711.
[5] Zhang H, Hu D, Peng H, Yuan W, Yang Z. In-plane crushing behavior and energy absorption of sponge-inspired lattice structures. Int J Mech Sci 2024;274:109328. https://doi.org/10.1016/j.ijmecsci.2024.109328.
[6] Niu Y, Du T, Liu Y. Biomechanical characteristics and analysis approaches of bone and bone substitute materials. J Funct Biomater 2023;14. https://doi.org/10.3390/jfb14040212.
[7] Morgan EF, Unnikrisnan GU, Hussein AI. Bone mechanical properties in healthy and diseased states. Annu Rev Biomed Eng 2018;20:119–43. https://doi.org/10.1146/annurev-bioeng-062117-121139.
[8] Jain T, Jyoti Minku, Sharma GK, Ghosh R. Design of functionally graded porous lattice structure tibial implant for TAR. Int J Mech Sci 2024;281:109671. https://doi.org/10.1016/j.ijmecsci.2024.109671.
[9] Chen Q, He Y, Lai S, Qi J, Zhang S, Jia S, et al. 3D characterization of vascular bundle in moso bamboo node and its effect on compressive properties. Holzforschung 2023;77:368–77. https://doi.org/10.1515/hf-2022-0177.
[10] Ahmad M, Kamke FA. Analysis of Calcutta bamboo for structural composite materials: physical and mechanical properties. Wood Sci Technol 2005;39:448–59. https://doi.org/10.1007/s00226-005-0016-y.
[11] Wang S, Deng C, Ojo O, Akinrinlola B, Kozub J, Wu N. Design and modeling of a novel three dimensional auxetic reentrant honeycomb structure for energy absorption. Compos Struct 2022;280:114882. https://doi.org/10.1016/j.compstruct.2021.114882.
[12] Miao X, Hu J, Xu Y, Su J, Jing Y. Review on mechanical properties of metal lattice structures. Compos Struct 2024;342:118267. https://doi.org/10.1016/j.compstruct.2024.118267.
[13] Andrew JJ, Schneider J, Ubaid J, Velmurugan R, Gupta NK, Kumar S. Energy absorption characteristics of additively manufactured plate-lattices under low-velocity impact loading. Int J Impact Eng 2021;149:103768. https://doi.org/10.1016/j.ijimpeng.2020.103768.
[14] Li L, Yang F, Jin Y, Li P, Zhang S, Xue K, et al. Multifunctional hybrid plate lattice structure with high energy absorption and excellent sound absorption. Mater Des 2024;241:112946. https://doi.org/10.1016/j.matdes.2024.112946.
[15] Cui Z, Zhao J, Xu R, Ding Y, Sun Z. Mechanical design and energy absorption performances of novel plate-rod hybrid lattice structures. Thin-Walled Structures 2024;194:111349. https://doi.org/10.1016/j.tws.2023.111349.

[16] Krešić I, Kaljun J, Rašović N. Controlling the mechanical response of stochastic lattice structures utilizing a design model based on predefined topologic and geometric routines. Applied Sciences 2024:14. https://doi.org/10.3390/app14146048.
[17] Korshunova N, Papaioannou I, Kollmannsberger S, Straub D, Rank E. Uncertainty quantification of microstructure variability and mechanical behavior of additively manufactured lattice structures. Comput Methods Appl Mech Eng 2021;385:114049. https://doi.org/10.1016/j.cma.2021.114049.
[18] Maliaris G, Sarafis E. Mechanical behavior of 3D printed stochastic lattice structures. Materials structure & micromechanics of fracture viii, 258. Trans Tech Publications Ltd; 2017. p. 225–8. https://doi.org/10.4028/www.scientific.net/SSP.258.225.
[19] Maskery I, Aremu AO, Simonelli M, Tuck C, Wildman RD, Ashcroft IA, et al. Mechanical properties of Ti-6Al-4V selectively laser melted parts with body-centred-cubic lattices of varying cell size. Exp Mech 2015;55:1261–72. https://doi.org/10.1007/s11340-015-0021-5.
[20] Jadhav Y, Berthel J, Hu C, Panat R, Beuth J, Barati Farimani A. Generative lattice units with 3D diffusion for inverse design: GLU3D. Adv Funct Mater 2024;34:2404165. https://doi.org/10.1002/adfm.202404165.
[21] Kolken HMA, Zadpoor AA. Auxetic mechanical metamaterials. RSC Adv 2017;7:5111–29. https://doi.org/10.1039/C6RA27333E.
[22] Abueidda DW, Bakir M, Abu Al-Rub RK, Bergström JS, Sobh NA, Jasiuk I. Mechanical properties of 3D printed polymeric cellular materials with triply periodic minimal surface architectures. Mater Des 2017;122:255–67. https://doi.org/10.1016/j.matdes.2017.03.018.
[23] Zadpoor AA. Mechanical meta-materials. Mater Horiz 2016;3:371–81. https://doi.org/10.1039/C6MH00065G.
[24] Babaee S, Shim J, Weaver JC, Chen ER, Patel N, Bertoldi K. 3D Soft metamaterials with negative poisson's ratio. Adv Mater 2013;25:5044–9. https://doi.org/10.1002/adma.201301986.
[25] Liu Y. Mechanical properties of a new type of plate–lattice structures. Int J Mech Sci 2021;192:106141. https://doi.org/10.1016/j.ijmecsci.2020.106141.
[26] Kim Y, Kim Y, Yang C, Park K, Gu GX, Ryu S. Deep learning framework for material design space exploration using active transfer learning and data augmentation. NPJ Comput Mater 2021;7:140. https://doi.org/10.1038/s41524-021-00609-2.
[27] Guo K, Yang Z, Yu C-H, Buehler MJ. Artificial intelligence and machine learning in design of mechanical materials. Mater Horiz 2021;8:1153–72. https://doi.org/10.1039/D0MH01451F.
[28] Hsu Y-C, Yu C-H, Buehler MJ. Tuning mechanical properties in polycrystalline solids using a deep generative framework. Adv Eng Mater 2021;23:2001339. https://doi.org/10.1002/adem.202001339.
[29] Peng B, Wei Y, Qin Y, Dai J, Li Y, Liu A, et al. Machine learning-enabled constrained multi-objective design of architected materials. Nat Commun 2023;14:6630. https://doi.org/10.1038/s41467-023-42415-y.
[30] Mao Y, He Q, Zhao X. Designing complex architectured materials with generative adversarial networks. Sci Adv 2024;6:eaaz4169. https://doi.org/10.1126/sciadv.aaz4169.
[31] Challapalli A, Li G. Machine learning assisted design of new lattice core for sandwich structures with superior load carrying capacity. Sci Rep 2021;11:18552. https://doi.org/10.1038/s41598-021-98015-7.
[32] Hu Z, Ding J, Ding S, Ma WWS, Chua JW, Li X, et al. Machine learning – enabled inverse design of shell-based lattice metamaterials with optimal sound and energy absorption. Virtual Phys Prototyp 2024;19:e2412198. https://doi.org/10.1080/17452759.2024.2412198.
[33] Zeng Q, Duan S, Zhao Z, Wang P, Lei H. Inverse design of energy-absorbing metamaterials by topology optimization. Adv Sci (Weinh) 2023;10:e2204977. https://doi.org/10.1002/advs.202204977.
[34] Dold D, Aranguren van Egmond D. Differentiable graph-structured models for inverse design of lattice materials. Cell Rep Phys Sci 2023;4:101586. https://doi.org/10.1016/j.xcrp.2023.101586.
[35] Meyer PP, Tancogne-Dejean T, Mohr D. Non-symmetric plate-lattices: recurrent neural network-based design of optimal metamaterials. Acta Mater 2024;278:120246. https://doi.org/10.1016/j.actamat.2024.120246.
[36] Zong Z, Wen P, Chai Z, Wu D, Ding H, Wu Z. Deep learning-assisted design of mechanical metamaterials. Adv. Intell Discovery 2025:202500084. https://doi.org/10.1002/aidi.202500084. n/a.
[37] Brock A, Donahue J, Simonyan K. Large scale GAN training for high fidelity natural image synthesis. Advances in neural information processing systems, 32. Curran Associates, Inc.; 2019. p. 4407–20. NeurIPS 2019.
[38] Goodfellow IJ, Pouget-Abadie J, Mirza M, Xu B, Warde-Farley D, Ozair S, et al. Generative adversarial nets. editors. In: Ghahramani Z, Welling M, Cortes C, Lawrence N, Weinberger KQ, editors. Adv neural inf process syst. Curran Associates, Inc.; 2014. vol. 27.
[39] Kingma, D.P., & Welling M. Auto-encoding variational bayes. 2013.
[40] Rezende DJ, Mohamed S. Variational inference with normalizing flows. In: International Conference on Machine Learning (ICML); 2015. p. 37. 2015.
[41] Song Y, Ermon S. Score-based generative modeling through stochastic differential equations. In: Proceedings of the 37th International Conference on Machine Learning (ICML); 2020.
[42] Wang L, Chan Y-C, Ahmed F, Liu Z, Zhu P, Chen W. Deep generative modeling for mechanistic-based learning and design of metamaterial systems. Comput Methods Appl Mech Eng 2020;372:113377. https://doi.org/10.1016/j.cma.2020.113377.
[43] Bastek J-H, Kumar S, Telgen B, Glaesener RN, Kochmann DM. Inverting the structure–property map of truss metamaterials by deep learning. Proc. Natl Acad Sci 2022;119:e2111505119. https://doi.org/10.1073/pnas.2111505119.
[44] Raissi M, Perdikaris P, Karniadakis GE. Physics-informed neural networks: a deep learning framework for solving forward and inverse problems involving nonlinear partial differential equations. J Comput Phys 2019;378:686–707. https://doi.org/10.1016/j.jcp.2018.10.045.
[45] Karniadakis GE, Kevrekidis IG, Lu L, Perdikaris P, Wang S, Yang L. Physics-informed machine learning. Nature Reviews Physics 2021;3:422–40.
[46] Bian Y, Wang R, Yang F, Li P, Song Y, Feng J, et al. Mechanical properties of internally hierarchical multiphase lattices inspired by precipitation strengthening mechanisms. ACS Appl Mater Interfaces 2023;15:15928–37. https://doi.org/10.1021/acsami.2c20063.
[47] Li P, Yang F, Liu Y, Bian Y, Zhang S, Wang L, et al. Design of dual-phase lattice materials with balanced modulus, strength and energy absorption properties based on Sudoku arranged reinforcement phase distribution. Comput Struct 2023;286:107093. https://doi.org/10.1016/j.compstruc.2023.107093.
[48] Jin L, Yu S, Cheng J, Ye H, Zhai X, Jiang J, et al. Machine learning driven forward prediction and inverse design for 4D printed hierarchical architecture with arbitrary shapes. Appl Mater Today 2024;40:102373. https://doi.org/10.1016/j.apmt.2024.102373.
[49] Shang X, Liu Z, Zhang J, Lyu T, Zou Y. Tailoring the mechanical properties of 3D microstructures: a deep learning and genetic algorithm inverse optimization framework. Materials Today 2023;70:71–81. https://doi.org/10.1016/j.mattod.2023.09.007.
[50] Deb K, Anand A, Joshi D. A computationally efficient evolutionary algorithm for real-parameter optimization. Evol Comput 2002;10:371–95. https://doi.org/10.1162/106365602760972767.
[51] Wang Y, Zeng Q, Wang J, Li Y, Fang D. Inverse design of shell-based mechanical metamaterial with customized loading curves based on machine learning and genetic algorithm. Comput Methods Appl Mech Eng 2022;401:115571. https://doi.org/10.1016/j.cma.2022.115571.
[52] Wang X, Xu S, Zhou S, Xu W, Leary M, Choong P, et al. Topological design and additive manufacturing of porous metals for bone scaffolds and orthopaedic implants: a review. Biomaterials 2016;83:127–41. https://doi.org/10.1016/j.biomaterials.2016.01.012.
[53] Oryan A, Alidadi S, Moshiri A, Maffulli N. Bone regenerative medicine: classic options, novel strategies, and future directions. J Orthop Surg Res 2014;9:18. https://doi.org/10.1186/1749-799X-9-18.
[54] O'Brien FJ. Biomaterials & scaffolds for tissue engineering. Materials Today 2011;14:88–95. https://doi.org/10.1016/S1369-7021(11)70058-X.
[55] Peng B, Wei Y, Qin Y, Dai J, Li Y, Liu A, et al. Machine learning-enabled constrained multi-objective design of architected materials. Nat Commun 2023;14:1–12. https://doi.org/10.1038/s41467-023-42415-y.
[56] Minami M, Yoshikawa K, Matsuoka Y, Itai Y, Kokubo T, Iio M. MR study of normal joint function using a low field strength system. J Comput Assist Tomogr 1991;15.
[57] Di Frisco G, Yousefi Nooraie R, Guagliano M, Bagherifard S. Structural design and characterization of hybrid hierarchical lattice structures based on sheet-network triply periodic minimal surface topology. Mater Des 2024;246:113336. https://doi.org/10.1016/j.matdes.2024.113336.
[58] Tancogne-Dejean T, Diamantopoulou M, Gorji MB, Bonatti C, Mohr D. 3D Plate-lattices: an emerging class of low-density metamaterial exhibiting optimal isotropic stiffness. Advanced Materials 2018;30:1803334. https://doi.org/10.1002/adma.201803334.
[59] Berger JB, Wadley HNG, McMeeking RM. Mechanical metamaterials at the theoretical limit of isotropic elastic stiffness. Nature 2017;543:533–7. https://doi.org/10.1038/nature21075.
[60] Yazdani Sarvestani H, Akbarzadeh AH, Mirbolghasemi A, Hermenean K. 3D printed meta-sandwich structures: failure mechanism, energy absorption and multi-hit capability. Mater Des 2018;160:179–93. https://doi.org/10.1016/j.matdes.2018.08.061.
[61] Wang X, Zhang L, Song B, Zhang J, Fan J, Zhang Z, et al. Anisotropic mechanical and mass-transport performance of Ti6Al4V plate-lattice scaffolds prepared by laser powder bed fusion. Acta Biomater 2022;148. https://doi.org/10.1016/j.actbio.2022.06.016.
[62] Yu G, Xiao L, Song W. Deep learning-based heterogeneous strategy for customizing responses of lattice structures. Int J Mech Sci 2022;229:107531. https://doi.org/10.1016/j.ijmecsci.2022.107531.
[63] Mora Sierra DC, Heydari Astaraee A, Guagliano M, Bagherifard S. Numerical investigation of Ti6Al4V gradient lattice structures with tailored mechanical response. Adv Eng Mater 2022;24:2101760. https://doi.org/10.1002/adem.202101760.